PERGAMON

International Journal of Heat and Mass Transfer 41 (1998) 2967–2977

International Journal of HEAT and MASS TRANSFER

Theoretical study of heat and mass transfer in a zeolite bed during water desorption: validity of local thermal equilibrium assumption

A. Mhimid

Département de Génie Energétique, Ecole Nationale d'Ingénieurs de Monastir, 5000 Monastir, Tunisia

Received 20 June 1997; in final form 8 December 1997

Abstract

We have studied heat and mass transfer in a zeolite bed during water desorption. For this purpose, a mathematical model based on scale changing has been established. We have tested the local thermal equilibrium assumption in a two-dimensional flow.

The problem is numerically resolved using a finite volume method. The numerical simulation gives the time and space evolution of temperature and moisture content. The influence of different effects (essentially the effective conductivity of the solid and the reactor geometry) on the total mass desorbed are examined.

Key words: Zeolithe; Desorption; Kinetic; Moisture content; Bidimensional; Numerical resolution; Finite volume.

Nomenclature

C_p specific heat [J kg^{-1} K^{-1}]
d_p mean particle diameter [m]
h heat transfer coefficient between the bed and the heating source [W m^{-2}]
h_{gs} heat transfer coefficient between solid and gas [W m^{-2}]
h_0 heat transfer coefficient between the bed and the outlet of the gas [W m^{-2}]
H height of the bed [m]
K permeability [m^2]
m evaporation rate [kg m^{-3} s^{-1}]
P pressure [Pa]
Pr Prandtl number
r radial coordinate [m]
R ray of the bed drying [m]
Re Reynolds number
S solid–gas transfer area [m^2 m^{-3}]
t time [s]
T temperature [K]
V gas velocity [m s^{-1}]
X moisture content
z axial coordinate [m].

Greek symbols

ΔH latent heat of vaporization [J kg^{-1}]
Δr radial depth increment [m]
Δz longitudinal depth increment [m]
Δt time increment [s]
ε bed porosity
λ thermal conductivity [W m^{-1} K^{-1}]
λ^* effective thermal conductivity [W m^{-1} K^{-1}]
ρ density [kg m^{-3}]
ω volume [m^3].

Subscripts

c condenser
eq equilibrium
g gas
ge gas effective
h heating
i initial
j constituent
m, n spatial indices
s solid
se solid effective
sat saturation

0017–9310/98 $19.00
PII: S0017-9310(98)00010-6

v vapor
vap vaporization.

1. Introduction

The zeolite–water reactor has been used in many installations. Applications of adsorption system including solar cooling, energy storage, automobile and residential space conditioning have been reported [1–7]. A knowledge of heat and mass transfer in the reactor during the water sorption by zeolite is very important for reactor optimization. Several attempts have been made to analyze the sorption phenomena and chemical sorption [6–14]. In these studies, the models assumed that the gas and the solid temperatures are equal (validity of equilibrium local thermal) and the transfer is a one-dimensional process. The two-dimensional model is used by Hajji and Khalloufi [10]. We have established a mathematical model for energy transport [15] based on the two phases equation model which assumes no local thermal equilibrium between the fluid and the solid phases. The same assumption has been used previously to study heat and mass transfer during chemical sorption [16, 17].

In all these different models, the principal idea consists of:

(i) two temperatures (gas, solid) or one temperature are considered in the medium;
(ii) pressure is constant or variable;
(iii) one-dimensional or two-dimensional transfers.

The validity of these assumptions is not yet completely studied. In this paper, we report the results of heat and mass transfer during water desorption by zeolite and we address:

—the local thermal equilibrium assumption;
—the two-dimensional transfer.

Two mathematical models based on scale changing, have been established, to study heat and mass transfer in a zeolite bed during water desorption. The solution of the system of equations has been obtained numerically by the finite volume method [18]. The numerical simulation gives the time and space evolution of the temperatures and moisture content. Different effects are examined such as the effective conductivity of the solid and the reactor geometry, on the total mass desorbed. Also, the validity of the local thermal equilibrium (LTE) has been discussed.

2. Formulation of heat and mass transfer

The cylindrical reactor, considered in this paper, exchanges heat through lateral and base area at a constant temperature and a constant flow rate heating fluid (Fig. 1). The reactor is composed of a solid phase (zeolite and water) and a gaseous phase (vapor) so it is a discontinuous medium. The equations which govern heat and mass transfer are generally obtained by changing the scale [19]. One passes from the microscopic view, in which the averaging volume is small compared to the pores, to the macroscopic view in which the averaging volume is large with regard to the pores. This scale changing enables us to convert the real discontinuous medium to a fictious continuous equivalent one. Each macroscopic term is obtained by averaging the microscopic one. The macroscopic differential equations are obtained by taking the average of the microscopic equations over the averaging volume which holds a lot of grains and by using closing assumptions. The microscopic equations are the equations of momentum, mass and energy conservation in all considered phases and at the interfaces. These equations are obtained by using thermodynamic and mechanic laws of continuous media.

Several assumptions are made in order to obtain a closed set of governing equations at macroscopic scale:

—the porous medium is homogeneous and isotropic;
—the porous particles are incompressible;
—the compression work and viscous dissipation are negligible;
—the inter-particle radiation is linearized and included in the heat exchange solid–gas coefficient and the solid thermal conductivity;
—the dispersion terms and the tortuosity terms can be modeled as diffusive fluxes;

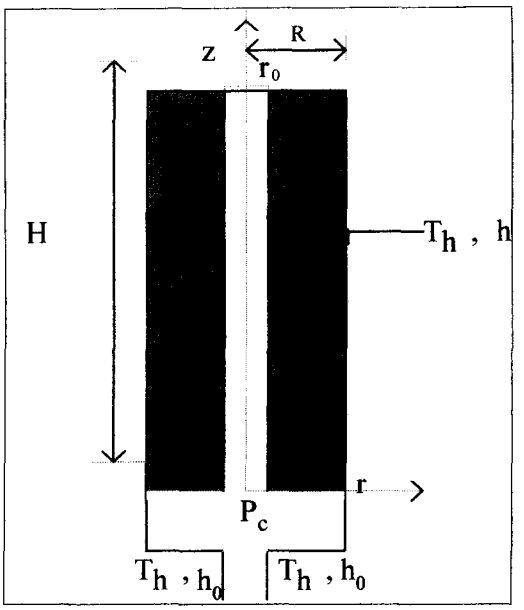

Fig. 1. Sketch of the fixed bed.

—the gas phase is ideal from the thermodynamic view point.

When the transfers are two dimensional and depend on the r and z axes, the governing equations become:

(1) Vapor mass conservation equation

$$\varepsilon\frac{\partial\rho_g}{\partial t}+\mathrm{div}(\rho_g V_g)-\dot{m}. \tag{1}$$

(2) Gas energy equation

$$\varepsilon\rho_g C_{pg}\frac{\partial T_g}{\partial t}+\rho_g V_g C_{pg}\,\mathrm{grad}(T_g)=\mathrm{div}\,[\varepsilon\lambda_{ge}\,\mathrm{grad}(T_g)]+C_{pg}\dot{m}[T_g-T_s]-H_{gs}S[T_g-T_s]. \tag{2}$$

(3) Solid energy equation

$$\rho C_p\frac{\partial T_s}{\partial t}=\mathrm{div}\,[(1-\varepsilon)\lambda_{se}\,\mathrm{grad}(T_s)]+\dot{m}\Delta H_{vap}+H_{gs}S[T_g-T_s] \tag{3}$$

where $\rho C_p=\rho_s(1-\varepsilon)[C_{ps}+XC_{pw}]$.

(4) Energy equation (when LTE is valid)

One of the assumptions made in many studies consist of considering T_g equal to T_s at any point (the medium is considered at local thermal equilibrium). Then, a single equation is sufficient to determine the temperature field in the reactor. To avoid exchange terms, this equation is obtained by adding equations (2) and (3).

$$[(1-\varepsilon)\rho_s(C_{ps}+XC_{pw})+\varepsilon\rho_g C_{pg}]\frac{\partial T}{\partial t}+\rho_g C_{pg}V_g\,\mathrm{grad}(T)=\dot{m}\Delta H_{vap}+\mathrm{div}\,[\lambda^*\,\mathrm{grad}(T)] \tag{4}$$

where $\lambda^*=(1-\varepsilon)\lambda_{se}+\varepsilon\lambda_{ge}$.

The model formed by equations (1), (2) and (3) on one hand and by the equations (1) and (4) on the other hand will be denoted in the remaining part of this paper as respectively NLTEModel and LTEModel.

(5) Momentum equation

The vapor velocity can be expressed by Darcy's law

$$V_g=-\frac{K}{\mu_g}\mathrm{grad}(P_g). \tag{5}$$

(6) Kinetic equation

The mass rate of evaporation is:

$$\dot{m}=-(1-\varepsilon)\rho_s\frac{\partial X}{\partial t} \tag{6}$$

where X is the moisture content:

$$\frac{dX}{dt}=-G(X-X_{eq\infty}). \tag{7}$$

The mass transfer coefficient G is obtained by estimation from experimental data [6]. In this equation the equilibrium moisture content X_{eq} is determined by Dubinin's equation [20]

$$X_{eq}=X_0\exp\left[-D\left(T_g\log\left(\frac{P_{sat}(T_g)}{P_v}\right)^2\right)\right] \tag{8}$$

where the coefficients X_0 and D are determined, experimentally, by Guilleminot [21].

2.1. Boundary and initial conditions

2.1.1. Initial conditions

Initially, the temperature, the pressure and the moisture content in the reactor are assumed to be constants:

$$T_g(0,r,z)=T_s(0,r,z)=T_i,\quad P_g(0,r,z)=P_i$$

and $$X(0,r,z)=X_i.$$

2.1.2. Pressure boundary conditions

At the outlet of the bed ($z=0$) the pressure is assumed constant:

$$P_g(t,r,0)=P_c.$$

At the base surface ($z=H$), at the lateral area ($r=R$), and at the inner surface ($r=r_0$), the wall is impervious:

$$\frac{\partial P_g}{\partial z}(t,r,H)=0 \tag{9}$$

$$\frac{\partial P_g}{\partial r}(t,R,z)=0 \tag{10}$$

$$\frac{\partial P_g}{\partial z}(t,r_0,z)=0. \tag{11}$$

2.1.3. Thermal boundaries conditions for the NLTEModel (when gas temperature and solid temperature are different)

At the outlet of the cylinder ($z=0$) the exchanges are not well known and the flow existing on the porous surface is very complex. In order to solve this problem correctly, it is necessary to extend the domain of computation to take into account fluid flow and heat transfer in the fluid near the upper surface. However, these conditions may complicate enormously this study. To avoid this problem, we have introduced in the case a heat transfer coefficient h_0. The effect of h_0 on the total mass transfer is negligible [15]

$$-\lambda_{se}\frac{\partial T_s}{\partial z}(t,r,0)=h_0(T_s-T_h) \tag{12}$$

$$-\lambda_{ge}\frac{\partial T_g}{\partial z}(t,r,0)=h_0(T_g-T_h). \tag{13}$$

The base area ($z=H$), and the lateral area ($r=R$) are heated with a constant temperature, we have also introduced a heat transfer coefficients h:

$$\text{for the solid:}\quad -\lambda_{se}\frac{\partial T_s}{\partial z}(t,r,H)=h(T_s-T_h) \tag{14}$$

$$-\lambda_{se}\frac{\partial T_s}{\partial r}(t,R,z)=h(T_s-T_h) \tag{15}$$

$$\text{for the gas:}\quad -\lambda_{ge}\frac{\partial T_g}{\partial z}(t,r,H)=h(T_g-T_h) \tag{16}$$

$$-\lambda_{ge}\frac{\partial T_g}{\partial z}(t, R, z) = h(T_g - T_h). \quad (17)$$

Taking a small r_0, the volume limited at the inner surface is supposed isothermal, we deduce that:

$$-\lambda_{se}\frac{\partial T_s}{\partial r}(t, r_0, z) = 0 \quad (18)$$

$$-\lambda_{ge}\frac{\partial T_g}{\partial r}(t, r_0, z) = 0. \quad (19)$$

2.2. For the LTEModel (local thermal equilibrium is valid)

Initially, the temperature is uniform: $T(0, r, z) = T_i$. At the outlet ($z = 0$) we have:

$$-\lambda^*\frac{\partial T}{\partial z}(t, r, 0) = h_0(T - T_h). \quad (20)$$

At the base area ($z = H$) and at the lateral area ($r = R$), considering T_g equal to T_s (validity of local thermal equilibrium) and adding equation (14) to equation (16), and equation (15) to equation (17) we obtain:

$$-\lambda^*\frac{\partial T}{\partial z}(t, r, H) = h(T - T_h) \quad (21)$$

$$-\lambda^*\frac{\partial T}{\partial z}(t, R, z) = h(T - T_h). \quad (22)$$

At the inner surface, we can write:

$$-\lambda^*\frac{\partial T}{\partial z}(t, r_0, z) = 0. \quad (23)$$

3. Numerical resolution

The system of the presented equations is solved numerically by the method of control volume as described by Patankar [19]. The advantage of this method ensures flux conservation, and thus avoids generation of parasitic sources. The method consists of defining a grid of points $P_{n,m}$ within the calculated domain and then constructing around each point a control volume (Fig. 2). The value

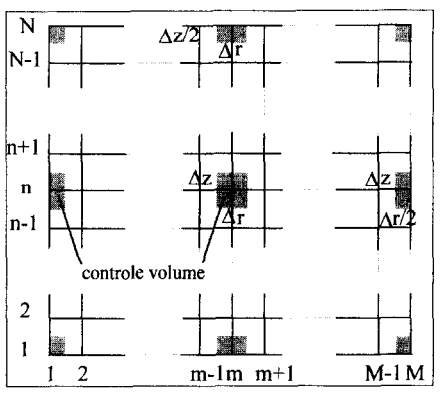

Fig. 2. Numerical grid.

of a physical quantity Ψ at any point $P_{n,m}$ and at the time $t+\Delta t$ will be noted $\Psi_{n,m}^{i+1}$. The equations are integrated over this control domain and over the interval of time $[t, t+\Delta t]$.

In order to discretize the resulting integral equations back to algebraic equations tying together the solution values at the nodes of the grid, we make the following assumption:

—the fluxes are constant on the face of the control volume which is perpendicular to them;
—the accumulation terms and the source terms can be approximated by averages on the control volume constructed around $P_{n,m}$.

To avoid numerical instabilities we have adopted an implicit scheme.

At the boundary limits of the bed, the equations are discretized by integrating over the half of the control volume and by taking into account the boundary conditions. At the corner we have used the quarter of the control volume.

The terms of transport by convection are discretized using an Upwind scheme. This scheme supposed that the values of convicted quantities at the face of the control volume are equal to their values at the grid point situated in the upstream.

The first derivatives, which are evaluated on the control volume faces, are approximated over two nodes within the porous medium using.

$$\left[\frac{\partial \Psi}{\partial z}\right]_{n+1/2,m}^{i+1} = \frac{\Psi_{n+1,m}^{i+1} - \Psi_{n,m}^{i+1}}{\Delta z}.$$

Considering these assumptions, the form of the resulting algebraic equations become:

$$A_0\Psi_{n,m}^{i+1} = A_w\Psi_{n,m-1}^{i+1} + A_e\Psi_{n,m+1}^{i+1} + A_s\Psi_{n-1,m}^{i+1} + A_n\Psi_{n+1,m}^{i+1} + A_1.$$

The resulting system of algebraic equation is solved numerically by the iterative line-by-line sweeping method. The choice of this method is justified by its rapid convergence compared to point by point methods. Scanning along the r axis, we set:

$$A_0\Psi_{n,m}^{i+1} = A_w\Psi_{n,m-1}^{i+1} + A_e\Psi_{n,m+1}^{i+1} + D$$

where

$$D = A_s\Psi_{n-1,m}^{i+1} + A_n\Psi_{n+1,m}^{i+1} + A_1.$$

This method solution consists in the evaluation using the predicted solution of A_0, A_w, A_e and D. Then, the tridiagonal resulting system of equations is solved by the standard Gaussian-elimination method. If the difference between the calculated and estimated solutions is small, the convergence to the solution is achieved, or else we repeat the procedure of evaluation of the coefficients using the solution which have already calculated until convergence.

4. Numerical data

The cylinder has an inner radius 0.03 m, an outer radius 0.1 m and a height 1.2 m. This cylinder filled with grains of zeolithe. The lateral area is heated by a constant temperature $T_h = 400$ K. It is connected to a condenser which has a constant temperature $T_c = 313$ K and a constant pressure $P_c = 70$ mbars.

The physical characteristics of the vapor and the zeolithe [4, 14, 23] are: $\varepsilon = 0.7$, $d_p = 2.510^{-3}$ m, $\rho_s = 1400$ kg m^{-3}, $\lambda^* = 0.2$ W m^{-1} K^{-1}, $C_{ps} = 836$ J kg^{-1} K^{-1}, $\lambda_{ge} = 0.024$ W m^{-1} K^{-1}, $C_{pg} = 1840$ J kg^{-1} K^{-1} and $C_{pe} = 4180$ J kg^{-1} K^{-1}.

Initially, the moisture content, the temperature and the pressure in the reactor are: $X_i = 0.266$ kg of water/kg of zeolithe, $T_i = 293$ K, $P_i = 6$ mbars.

The permeability and the specific surface area of the packed bed which appears in energy equations are [24, 25]:

$$K = \frac{\varepsilon^3 d_p^2}{150(1-\varepsilon)^2} \quad \text{and} \quad S = 6\frac{(1-\varepsilon)}{d_p}.$$

The heat transfer coefficient between solid and gas is given by [25]:

$$h_{gs} = \frac{\lambda_g}{d_p}(2 + 1.8 Pr^{0.33} Re^{0.5})$$

$$Re = \frac{\rho_g V_g d_p}{\mu_g}; \quad Pr = \frac{\mu_g C_{pg}}{\lambda_g}.$$

5. Results and discussion

5.1. Validation of the numerical simulation

The numerical simulation has been validated by comparison with experimental data [6] of a cylindrical solar collector. The cylinder has an inner radius 0.03 m, an outer radius 0.1 m and a height 1.2 m. The lateral area is heated by a solar energy. The temperature T_h is variable and takes the values measured. These values correspond to those of outer surface. In these conditions, we have a constant temperature $T_c = 313$ K and a constant pressure $P_c = 70$ mbars.

From the measurements of the day (17 October 1989), numerical and experimental values of temperature on the inner surface and that of the outer surface is given in Fig. 3. The difference between temperature calculated and the experimental values is less than 2°C.

The total mass desorbed calculated and the experimental values are plotted in Fig. 4. The two results obtained are very similar.

5.2. General description

The results of the numerical simulation are presented as a curve giving the space evolution of solid temperature

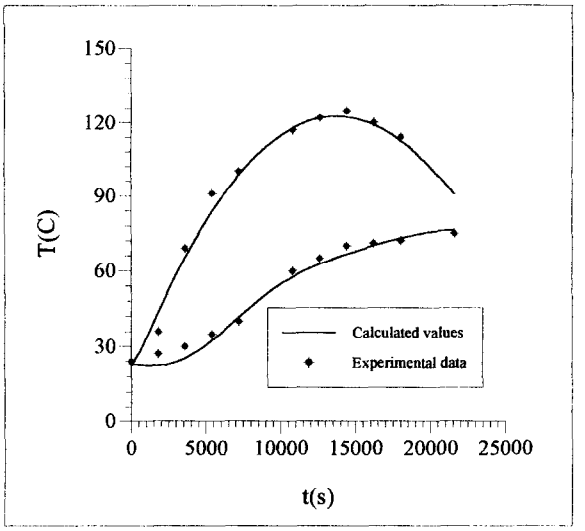

Fig. 3. Time evolution of the temperature at the inner and outer surface.

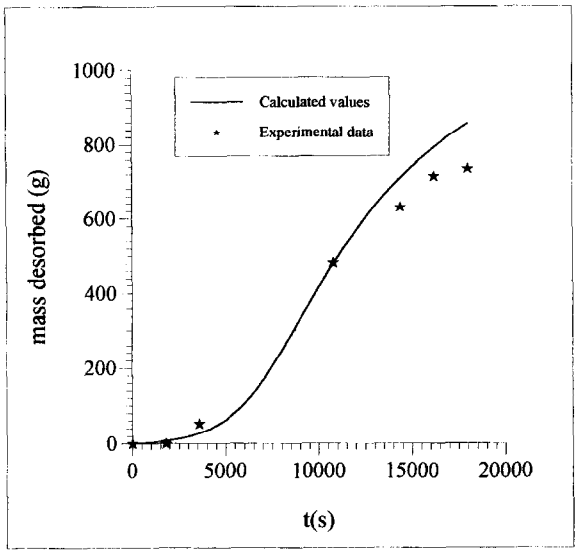

Fig. 4. Time evolution of the total mass desorbed.

(Fig. 5), and moisture content (Fig. 6) at different times ($t = 60$ s, $t = 3600$ s, $t = 28\,800$ s).

In these figures, we can see a front (Fig. 6) of desorption that moves with time and divides the bed in two regions (dried region and wet region). Evaporation is essentially localized in the zone in which the gradient of moisture content is high (front of evaporation). When time increases, the front of evaporation approaches in the center of the medium and the humid region contracts. After a large time, the moisture content tends to its equilibrium value and the mass rate is diminishing. After

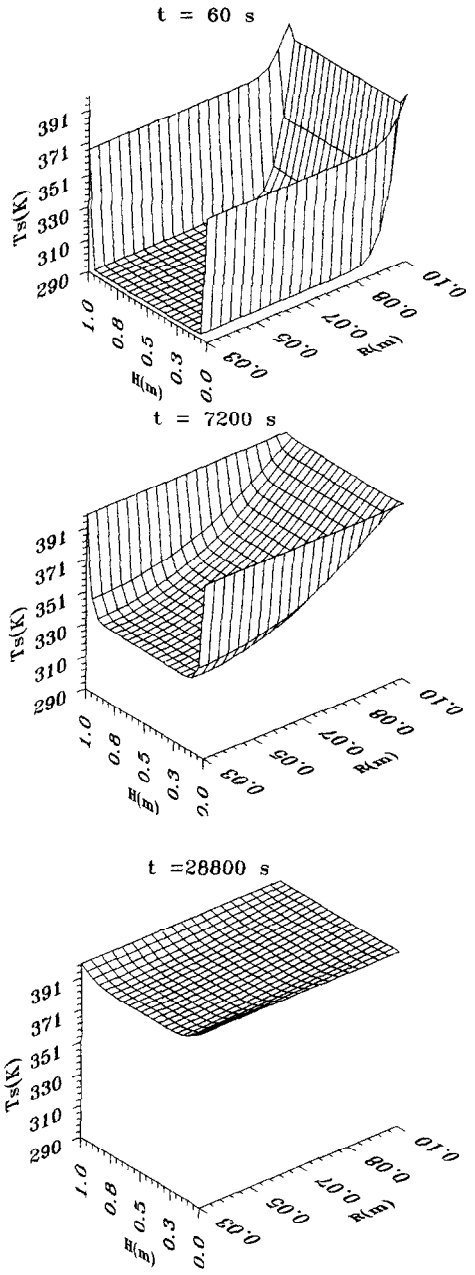

Fig. 5. Time–space evolution of solid temperature.

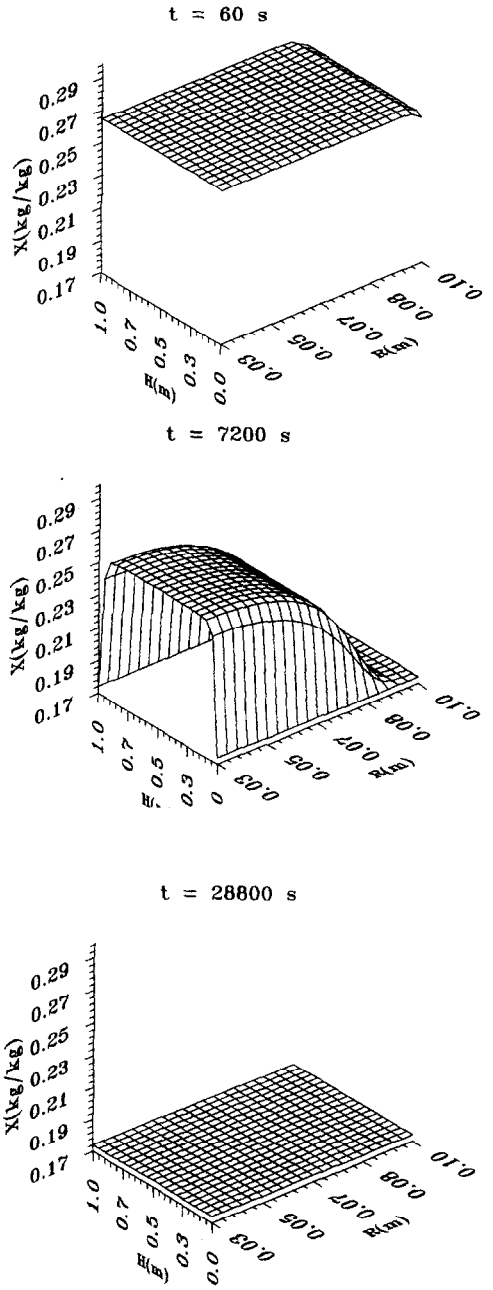

Fig. 6. Time–space evolution of moisture content.

an important period of time, the remaining quantity of moisture content in the reactor becomes too small.

We can notice that the desorption is more important near the lateral area than at the center. In fact, in this region, the temperature is greater than in the interior of the reactor. This situation is due to the external heating fluid (Fig. 5). When time increases, the overheating propagates inside the medium. At the end of desorption process, the solid temperature and the moisture content tend, respectively, to heating temperature and to the equilibrium moisture content.

5.3. *Validity of the local thermal equilibrium assumption*

—without desorption

Figure 7 shows the time–space evolution of the relative difference $|T_g - T_s|$ between solid temperature and gas

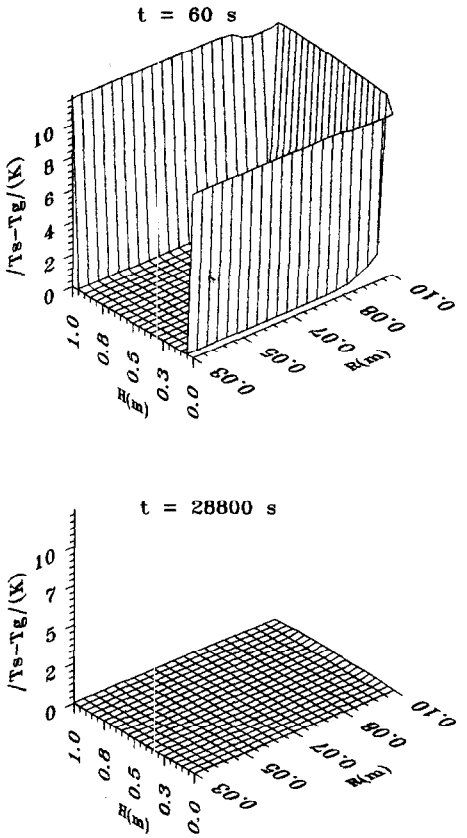

Fig. 7. Time–space evolution of the difference between solid temperature and gas temperature, without desorption.

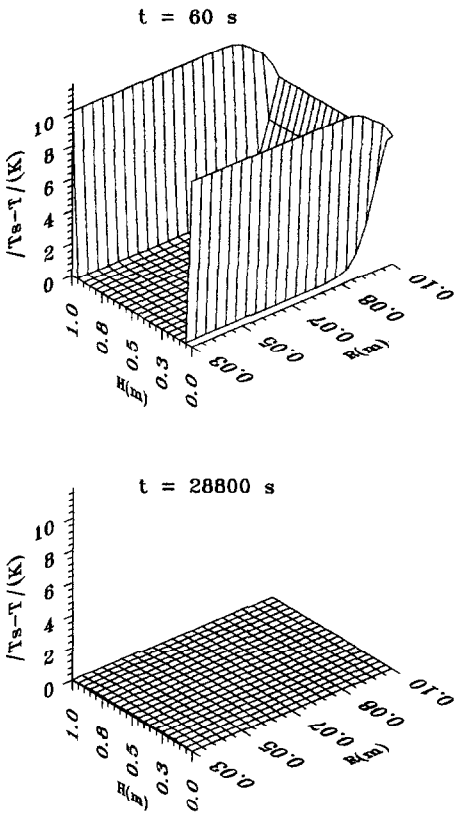

Fig. 8. Time–space evolution of the difference between solid temperature calculated by the two-temperature model and temperature calculated by the one-temperature model, without desorption.

temperature which is calculated without desorption with the NLTEModel. At the beginning, this difference is only important at the lateral area, because the heating temperature is higher than the initial medium temperature. After that, this difference decreases until zero.

Figure 8 shows the difference $|T-T_s|$ between the solid temperature calculated by the NLTEModel, and the temperature calculated by the LTEModel. The results obtained from the two models show an important discrepancy at the beginning. The difference $|T-T_s|$ decreases and advances in the bed. Except the first instants, the absolute and the relative value of the maximum difference between the local values of temperature calculated without desorption is very small (see Table 1). Consequently, the local thermal equilibrium assumption can be used.

—with desorption

Figure 9 shows the time–space evolution of the difference $|T_s-T_g|$ between solid temperature and gas temperature calculated, during the desorption, by the NLTE-Model. Figure 10 shows the time–space evolution of the difference $|T_s-T|$ between the solid temperature calculated by the NLTEModel and the temperature calculated by the LTEModel. We can see that within the reactor, the difference $|T_s-T_g|$ between the local temperature values calculated, when LTE is not valid, is negligible. However, near the outer wall the difference is in the order of 10 K for short times then decreases with time. This difference is due to the differences between the thermal characteristics of solid and the gas. As it has been reported previously [27, 28], the difference $|T_s-T_g|$ depends on the $\lambda_{se}/\lambda_{ge}$ and decreases when this ratio tends to unity.

The results of $|T_s-T_g|$ and $|T_s-T|$ obtained by using the two models are compared (see Table 2). We found that the absolute values of the temperature differences $|T_s-T|$ are higher than the absolute values of the difference between the solid and gas temperature $|T_s-T_g|$.

Figure 11 shows the time–space evolution of differences $|X_s-X|$ between the moisture contents using the two models. We can notice that the results are different in region corresponding to the front of vaporization. After desorption, this difference decreases to zero. Consequently, the total mass desorbed displays a small

Table 1
The absolute the relative value of the maximum difference between the local values of temperature calculated with desorption

Time [s]	$\lvert T_g - T_s \rvert$ [K]	$\lvert (T_g - T_s)/(T_h - T_i) \rvert$ [%]	$\lvert T - T_s \rvert$ (K)	$\lvert (T - T_s)/(T_h - T_i) \rvert$ [%]
60	11	10.28	10.38	9.70
3600	1.04	0.97	3.24	3.02
7200	0.471	0.44	3.33	3.11
18000	0.04	0.037	0.78	0.72
28800	0.009	0.008	0.22	0.20

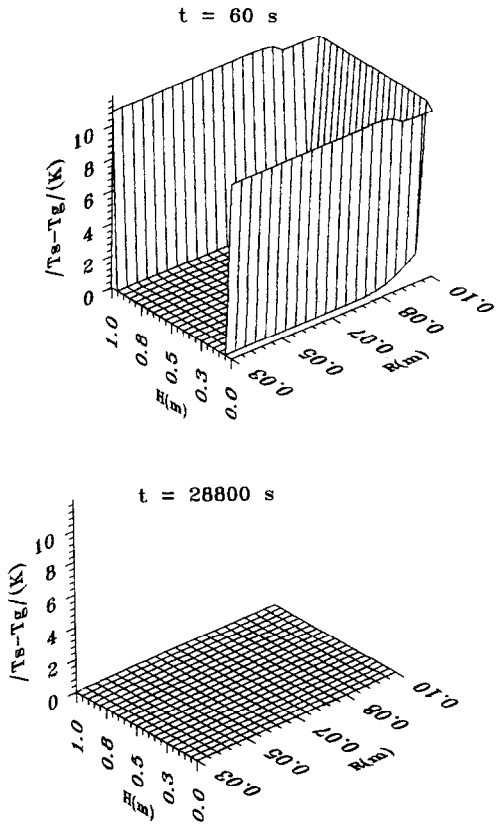

Fig. 9. Time–space evolution of the difference between solid temperature and gas temperature, with desorption.

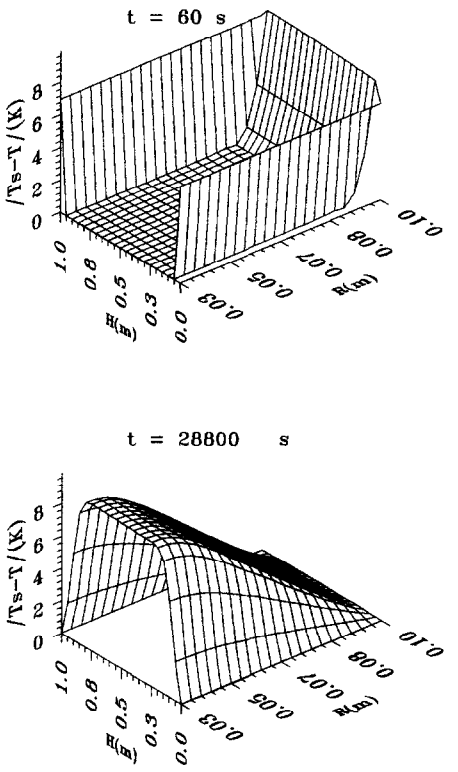

Fig. 10. Time–space evolution of the difference between solid temperature calculated by the two-temperature model and temperature calculated by the one-temperature model, with desorption.

difference at process middle (Fig. 12). At the end of desorption, the results tends to the same values.

5.4. Sensitivity to external conditions

Different effects such as the particle diameter, the constant desorption kinetic and the effective thermal conductivity are discussed. Sensitivity to external conditions such as the heating temperature, the outlet temperature, and heat coefficients are studied [15]. Here, we present the sensitivity of the reactor geometry and the effective thermal conductivity of the solid on the total mass desorbed.

(a) Sensitivity to the reactor geometry

The reactor volume, the physical characteristics and the boundary conditions were maintained constant during the simulation. The total mass desorbed is plotted for each reactor dimensions as a function of time (Fig. 13). We can note three zones:

For low values of H/R: the resistance to the transfers

Table 2
The absolute the relative value of the minimum difference between the local values of temperature calculated with desorption

Time [s]	$\lvert T_g - T_s \rvert$ [K]	$\lvert (T_g - T_s)/(T_h - T_i) \rvert$ [%]	$\lvert T - T_s \rvert$ (K)	$\lvert (T - T_s)/(T_h - T_i) \rvert$ [%]
60	11.77	11	7.55	7.05
3600	1.89	1.76	2.68	2.50
7200	1.21	1.13	4.34	4.05
18000	0.51	0.47	10.08	9.42
28800	0.24	0.22	12.70	11.87

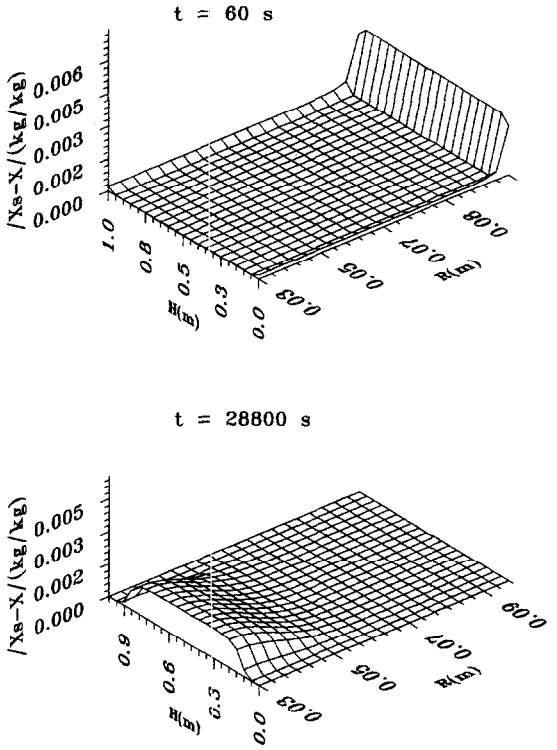

Fig. 11. Time–space evolution of the difference between moisture content calculated by the two-temperature model and moisture content calculated by the one-temperature model, with desorption.

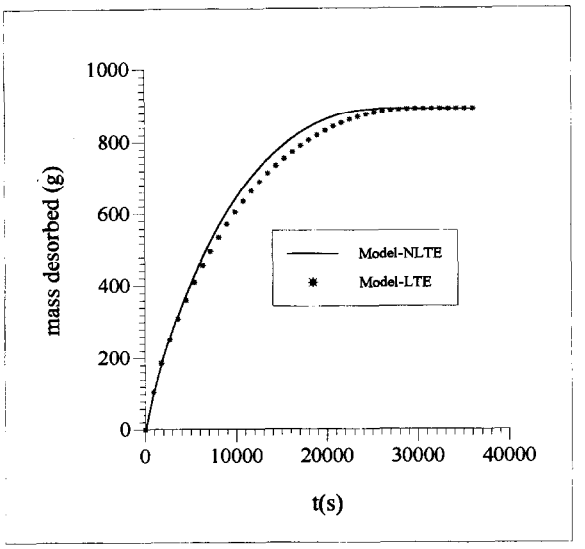

Fig. 12. Evolution of the total mass desorbed.

along r is higher. The heat and mass transfer in the reactor are one dimensional and depend only on z. Under these conditions, the resistance to the transfers along z direction increases when H/R increases; consequently, the total mass desorbed decreases.

For large values of H/R: the transfers are also one dimensional and depend only on r. When H/R rises the resistance to the transfers according to r decreases and the total mass desorbed increases.

For intermediate values of H/R: the two-dimensional effects are not negligible. When H/R increases the resistance to the transfers increases along the z direction and decreases along the radial direction. Those competing effects explain the existence of the minimum.

(b) Sensitivity to the effective thermal conductivity of the solid

For increasing the effective conductivity, several authors have been suggested the addition of wire or metal powder of high thermal diffusivity [26]. Thus it is of interest to study the effect of thermal conductivity on the heat and mass transfer. We have presented the time evolution of the total mass desorbed, for different values of effective conductivity (see Fig. 14) and the time of desorption as function of the effective solid conductivity (see Fig. 15). The numerical results give us that increasing the effective conductivity of the solid permits an acceleration of the desorption velocity. Increasing the thermal conductivity up to a value of about 5 W K^{-1} m^{-1} has no more significance. Choi and Mills [29] have studies this effect on hydrogen absorption. They show that the

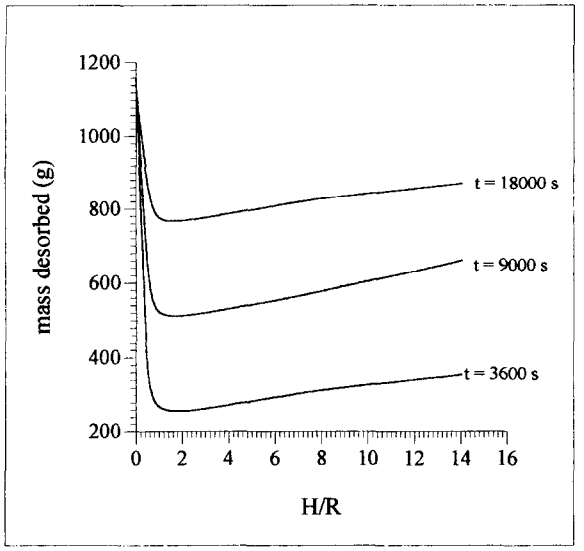

Fig. 13. Influence of the reactor geometry on the total mass desorbed.

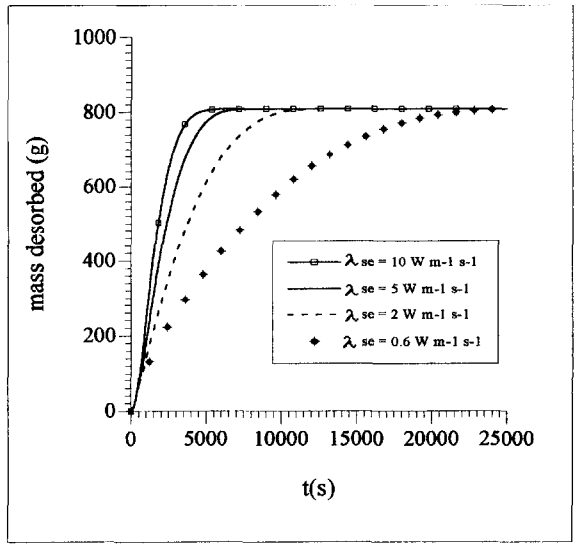

Fig. 14. Influence of the effective solid conductivity on the total mass desorbed.

increasing of the thermal conductivity up to a value of about 4 W K^{-1} m^{-1} gives a substantial improvement in the rate of the hydrogen absorption, whereas an increase above a value of about 5 W K^{-1} m^{-1} hydrogen flow and reaction kinetics become the rate limiting process. The same results were reported by Jemni and Ben Nasrallah [17].

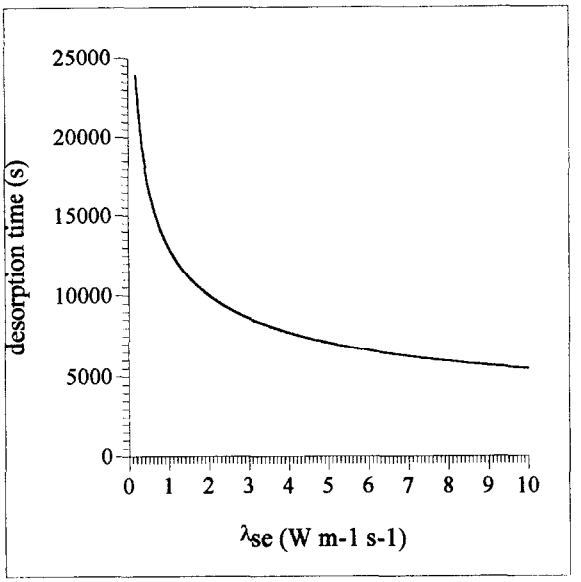

Fig. 15. Evolution of the time desorption.

6. Conclusion

Two numerical models for two-dimensional transient heat and mass transfer were established during water desorption by zeolite bed. These two numerical models allow us to determine the time–space evolution of states variables such as: temperature, moisture content. The local thermal equilibrium assumption is not valid on the heat point (at the wall, at the region where the vaporization takes place).

The LTEModel can be used to determine the total mass desorbed.

References

[1] Guillominot JJ, Meunier F. Etude expérimentale d'une glacière solaire utilisant le couple zeolithe 13X-eau. Rev Gen Therm, 1981.

[2] Shelton V. Solid adsorption heat pump system. United States patent. Patent no. 4 610 148. Date of Patent 9 September 1986.

[3] Meunier F. Réfrigération par adsorption. Revue Générale du Froid, 1982.

[4] Suzuki M. Application of adsorption cooling system to automobiles. In: International Institute of Refrigeration, editor. Proceedings of Commission BI of the IIR, Paris, 18–20 November 1992.

[5] Shelton SV. Residential space conditioning with solid sorption technology. In; International Institute of Refrigeration, editor. Proceedings of Commission BI of the IIR, Paris, 18–20 November 1992. pp. 67–76.

[6] Mhimid A. Etude expérimentale de la réfrigération solaire par adsorption utilisant des capteurs à zéolithe, plans et à

concentrations. Thèse de doctorat de Spécialité de l'Univerisité de Tunisie, 1991.

[7] Marmottant B, Mhimid A, El Golli S, Grenier P. Installation de réfrigération solaire par adsorption. Rev Gen Therm 1992;362:97–105.

[8] Ben Ammar N. Modélisation de pompes à chaleur à propagation de fronts de température. Thèse de Doctorat de l'Univerité de Technologie de Compiegna, 1993.

[9] Hajji A, Khallouji S. Theoretical and experimental investigation of a constant-pressure adsorption process. Int J Heat Mass Transfer 1995;38(18):3349–58.

[10] Hajji A, Khalloufi S. Improving the performance of adsorption heat exchangers using a finned structure. Int J Heat Mass Transfer 1996;39(8):1686–77.

[11] Sun LM. Modeling and simulation of nonisothermal and nonequilibrium multicomponent fixed bed dynamics. In: Meuner F, Levan MD, editors. Adsorption Processes for Gas Separation, Vol. 5. Paris (France), 1991. pp. 185–90.

[12] Lebrun M, Spinner B. Modélisation, simulation et dimensionnement d'un prototype à chaleur chimique solide–gaz. Entropie 1990;156:59–72.

[13] Boussehain, R, Feidt, ML. Caractérisation thermostatique de couples charbons actifs—Alcool, Incidence sur les critères de choix associées aux machines à quatre sources de chaleur JITH, Rabat 1985, pp. 137–45.

[14] Park I, Knaebel KS. Adsorber dynamics: stress associated with swelling and shrinkage. In: Meunier F, Levan MD. Adsorption Processes for Gas Separation, Vol. 5. Paris (France) 1991, pp. 191–6.

[15] Mhimid A, Jemni A, Ben Nasrallah S. Etude théorique des transferts couplés de chaleur et de masse lors de la désorption du couple zéolithe–eau. Rev Gen Therm 1997;36:697–706.

[16] Mir R, Bendou A, Zrikem Z, Gonzalez A. Etude des transferts de chaleur et de matière dans un réacteur solide/gaz par la méthode des éléments finis. Actes de la duexième Conférence Maghrébine de Génie des Procèdes. Tunisie 22–25 Avril 1996. pp. 355–8.

[17] Jemni A, Ben Nasrallah S. Study of two-dimensional heat and mass transfer during desorption in metal–hydrogen reacteur. Int J Hydrogen Energy 1995;20(11):881–91.

[18] Patankar S. Numerical Heat Transfer and Fluid Flow. New York: McGraw-Hill Company, 1980.

[19] Whitaker S. Simultaneous heat, mass and momentum transfers in porous media. A theory of drying. Advances of Heat Transfer 1977;13:119–203.

[20] Dubinin MM, Palavnik GM. Microporous of carbonaceous adsorbents. Carbon 1968;6.

[21] Guilleminot JJ. Caractérisation de l'état stationnaire liquide–gaz adsorbant lors de l'adsorption de gaz condensable sur le zéolithes Thèse de doctorat, Dijon (France): Université de Dijon, 1978.

[22] Abdallah K. Contribution expérimentale à l'étude de la cinétique d'adsorption de gaz. Thèse de doctorat de l'ENSAM, Paris (France), 1989.

[23] Sahnoune H. Mesure de la conductivé thermique d'une zéolithe supportée. Thèse de doctorat de l'Ecole Nationale Supérieure d'Arts et Métiers (France), 1988.

[24] Ranz WE. Friction and transfer coefficients for single particles and packed beds. Chemical Engineering Progress 1952;48(5):247–53.

[25] Bejan A. Convection Heat Transfer. New York: John Wiley and Sons, 1984.

[26] Mauran S, Prades P, L'Haridon F. Heat and mass transfer in consolidated reacting beds for thermochemican systems. In: International Institute of Refrigeration, editor. Proceedings of Commission BI of the IIR, Paris, 18–20 November 1992. pp. 259–265.

[27] Ben Nasrallah S, Amara T, Dupeuty MA. Convection naturelle instantionnaire dans un cylindre de grains ouvert à ses extremités et dont la paroi est chauffée par un flux de chaleur constant: validité de l'hypotheses de l'équilibre thermique local. Int J Heat Mass Transfer 1997;40(4):1155–68.

[28] Combarnous M, Bories S. Hydrothermal convection in saturated porous media. Adv Hydrosci 1975;10:231–307.

[29] Choi H. and Mills AF. Heat and mass transfer in metal hydride beds for heat pump applications. Int J Heat Mass Transfer 1990;33(6):1281–88.